THE JOURNAL OF BIOLOGICAL CHEMISTRY VOL. 280, NO. 48, pp. 40235–40240, December 2, 2005

Direct Observation of Protein Folding, Aggregation, and a Prion-like Conformational Conversion*

Received for publication, June 10, 2005, and in revised form, September 26, 2005 Published, JBC Papers in Press, October 3, 2005, DOI 10.1074/jbc.M506372200

Feng Ding[‡], **Joshua J. LaRocque**[‡§], **and Nikolay V. Dokholyan**[‡1]

From the [‡]*Department of Biochemistry and Biophysics, University of North Carolina School of Medicine , Chapel Hill, North Carolina 27599 and the* [§]*Department of Physics and Astronomy, University of North Carolina, Chapel Hill, North Carolina 27599*

Protein conformational transition from α-helices to β-sheets precedes aggregation of proteins implicated in many diseases, including Alzheimer and prion diseases. Direct characterization of such transitions is often hindered by the complicated nature of the interaction network among amino acids. A recently engineered small protein-like peptide with a simple amino acid composition features a temperature-driven α-helix to β-sheet conformational change. Here we studied the conformational transition of this peptide by molecular dynamics simulations. We observed a critical temperature, below which the peptide folds into an α-helical coiled-coil state and above which the peptide misfolds into β-rich structures with a high propensity to aggregate. The structures adopted by this peptide during low temperature simulations have a backbone root mean square deviation less than 2 Å from the crystal structure. At high temperatures, this peptide adopts an amyloid-like structure, which is mainly composed of coiled anti-parallel β-sheets with the cross-β-signature of amyloid fibrils. Most strikingly, we observed conformational conversions in which an α-helix is converted into a β-strand by proximate stable β-sheets with exposed hydrophobic surfaces and unsaturated hydrogen bonds. Our study suggested a possible generic molecular mechanism of the template-mediated aggregation process, originally proposed by Prusiner (Prusiner, S. B. (1998) *Proc. Natl. Acad. Sci. U. S. A.* 95, 13363–13383) to account for prion infectivity.

Protein conformation diseases, including Alzheimer, Lou Gehrig, and prion diseases (1), involve the aggregation of soluble proteins into insoluble amyloid fibrils following major conformational rearrangements. It has been shown that the amyloid fibrils formed by various proteins share a common core structure mainly composed of β-sheets (2). Thus, an intriguing conformational transition from α-helices to β-sheets occurs *en route* to the aggregation of natively α-helical proteins, such as prion proteins (3) in Creutzfeldt-Jakob disease and the Aβ peptide in Alzheimer disease (4). Understanding the molecular mechanism of such a transition is vital for the development of the final cure of amyloidogenic diseases (1).

Despite the importance of this type of conformational transition, the detailed molecular mechanism is largely unknown. It has been shown that misfolded prion proteins are infectious even across species barriers (3). A template model proposed by Prusiner (3) explains prion infectivity. In this model, misfolded prions induce the conversion of nearby native prions to the misfolded state. However, the exact aggregation pathway and the driving forces have yet to be uncovered.

Studies of molecular mechanisms and pathways are often hindered by complex interaction networks among the amino acids and in some cases by the large sizes of proteins related to these diseases. It has been shown that aggregation into amyloid fibrils is a common property of polypeptides (5, 6). Therefore, simple proteins and peptide systems can serve as model systems for deciphering the general mechanism of the α-helix to β-sheet conformational transition (7).

Characterization of conformational transitions of polypeptides that undergo large secondary-structure rearrangements is experimentally challenging because the time scales of these conformational changes are often experimentally inaccessible. Thus, computational approaches are necessary to provide additional insights into the conformational dynamics underlying the drastic conformational changes that occur during protein aggregation (8–13). Peng and Hansmann (8) performed *in silico* studies of a short seven-residue model peptide that can form either an α-helix or a metastable β-strand. The authors (8) also observed a template-mediated β-sheet development, in which a pre-made, frozen β-strand aided the unfolding of an α-helix. To facilitate the conversion, the authors covalently connected the two peptides by a short polyglycine segment. Lipfert *et al.* (12) employed a reaction path annealing algorithm to study the misfolding and amyloid formation of a short seven-residue peptide from the yeast prion protein in the presence of pre-made β-sheets. In this algorithm, the initial and final states are fixed, and the energy is computed along the pathway by multiple constrained simulations. Malolepsza *et al.* (13) observed a prion-like propagation of *in silico* designed peptide sequences by using a coarse-grained protein model. These hypothetical peptide sequences were designed *in silico* to feature a metastable β-sheet state in addition to the α-helical ground state. These studies provide computational evidence for the template model of propagating conformational changes proposed by Prusiner (3) that explains the lethal infection of pathological prions. However, to enable the sampling of the vast available conformational spaces, these computational studies either constrain the peptide systems between the folded and misfolded peptides (8, 12) or "freeze" the misfolded template into a pre-assumed β-sheet aggregate (8, 12, 13) within the close proximity of the folded peptide. Thus, it is possible that these observed conformational inter-conversions are a result of the artificial biases present in the simulations. Hence, an unconstrained study of an experimentally characterized protein system is necessary to understand the α-helix to β-sheet transition and to directly "observe" the template hypothesis proposed by Prusiner (3).

Recently, Kammerer *et al.* (7) designed a simple 17-residue peptide named ccβ, SIRELEARIRELELRIG, which behaves as a molecular switch; at low temperatures ccβ folds into a coiled-coil native state trimer, although at elevated temperatures it forms amyloid fibrils. Here we study the conformational transitions of this *de novo* peptide *in silico*.

* This work was supported in part by Muscular Dystrophy Association Grant MDA3720, March of Dimes Birth Defect Foundation Research Grant 5-FY03-155, and a University of North Carolina Chapel Hill research council grant. The costs of publication of this article were defrayed in part by the payment of page charges. This article must therefore be hereby marked "*advertisement*" in accordance with 18 U.S.C. Section 1734 solely to indicate this fact.

[1] To whom correspondence should be addressed: Dept. of Biochemistry and Biophysics, University of North Carolina School of Medicine, Chapel Hill, NC 27599. Tel.: 919-843-2513; Fax: 919-966-2852; E-mail: dokh@med.unc.edu.

A benefit of using the ccβ peptide as the model system for an aggregation study is the simplicity of the amino acid composition; it lacks aromatic residues, prolines, and cysteines, and its polar residues are either positively charged arginine or negatively charged glutamic acid residues. Significantly, the ccβ peptide is protein-like because it folds into a well defined native structure. We employ discrete molecular dynamics (DMD)[2] (14–17) simulations to study the folding and aggregation of this *de novo* peptide system. Our simulations reproduce the experimentally determined native state trimer of ccβ (7). Our simulations also capture the experimentally observed dependence of the conformational transition upon temperature. The structure of the aggregates from simulations satisfies the constraints derived from the experimental data, although the detailed atomic structure differs from the model proposed by Kammerer *et al.* (7). Most strikingly, we observe in the course of simulations that several peptides form a β-sheet that acts as a template to convert an α-helix into a β-strand, in the absence of any artificial constraints (8, 12, 13). This provides direct support of the hypothesis by Prusiner (3) of the template-based aggregation scheme for prion proteins.

MATERIALS AND METHODS

Discrete Molecular Dynamics Simulations—We modeled the peptides by a "bead-on-a-string" model with beads representing the backbone and side-chain heavy atoms. Along the backbone, the model contains the nitrogen (N), prime carbon (C′), carbonyl oxygen (O), and α-carbon (C-α). In the side chain, we introduced up to three coarse-grained beads, β, γ, and δ or γ_2 beads, depending on the properties of the individual amino acid. The parameters of the protein model and interactions are described in detail elsewhere (18). We used the DMD algorithm to perform simulations on our model proteins (14, 18).

All-Atom Reconstruction—We added the side-chain atoms and backbone H atoms for each amino acid based on the coordinates of the N, C-α, C-β, and C′ atoms. We used a Monte Carlo algorithm to search in the rotamer space (19) for the optimal arrangement of side chains. The scoring function for rotamer optimization includes van der Waals, solvation, and hydrogen bond interactions. The van der Waals radii and interaction strengths come from the Cedar force field (20). We applied the solvation model of EEF1 (21), and we used the statistical potential for hydrogen bonds proposed by Kortemme *et al.* (22).

All-Atom Molecular Simulations Using Amber—We used Amber (23) to perform all-atom molecular dynamics simulations. We started with coarse-grained structures produced in DMD simulations and then performed all-atom reconstructions. We then solvated our atomically detailed protein within an octagonal box of water molecules cut off 10 Å away from the protein. We used an octagonal box in our simulations to reduce the number of water molecules and to increase the efficiency of computation. To reduce the finite size effect, we utilized periodic boundary conditions. Next, we performed simulations using the SANDER module of Amber7, including the initial energy minimization and equilibration steps that eliminate steric clashes between reconstructed atoms.

The actual production simulations began with a free energy minimization of the water molecules, whereas the protein was maintained fixed. Then we minimized the energy of the entire system. Next, we raised the temperature of the system to 300 K. Finally, by using the Berendsen thermostat (see Ref. 24) to maintain the temperature of the system and the SHAKE method to monitor protein positions, we performed the actual production simulations.

[2] The abbreviations are: DMD, discrete molecular dynamics; r.m.s.d., root mean square distance.

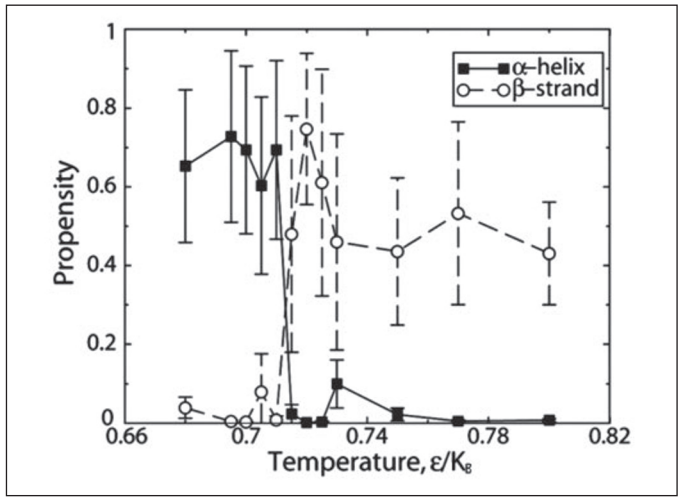

FIGURE 1. **The propensity of secondary structures, α-helices and β-strands, computed from equilibrium DMD simulations at various temperatures.** The secondary structure propensities at each temperature are averaged over all the residues, and the standard deviations are shown as *error bars*. A sharp transition of secondary structures occurs at $T_c = 0.71$.

Free Energy Calculation—We calculated the conformational free energies from the all-atom simulation trajectories by using the MM/PBSA (molecular mechanics/Poisson Boltzmann solvent-accessible surface area) module of Amber7 (25). We used the last nanosecond of each simulation to compute the conformational free energies. We took a snapshot each picosecond, and we collected 1000 snapshots for each simulation. The conformational free energy is the sum of the average gas phase (vacuum) energy (E_{GAS}), the average solvation energy (G_{SOL}), and the entropy ($-TS$). E_{GAS} included the electrostatics (E_{ELE}), the van der Waals (E_{VDW}), and the bonded energy (E_{INT}). The solvation free energy (G_{SOL}) included the electrostatic contribution G_{PB}, which we calculated with the Poisson-Boltzmann equation using FAMBE (26), and the nonpolar contribution, which is approximated as proportional to the solvent-accessible area (G_{SUR}) (25). The estimation of conformational entropy was very challenging (25). By using a quasi-harmonic approximation, we estimated the entropy from normal mode analysis with the NMODE module in Amber. We assumed T to be the room temperature 298.15 K.

RESULTS

Starting from extended and spatially separated ccβ peptides, we performed equilibrium DMD simulations over a range of temperatures. We first studied the folding and aggregation of three ccβ peptides. We also studied the aggregation process in high temperature simulations of six ccβ peptides. We modeled ccβ peptides by using four types of interactions as follows: hydrophobic (0.84ϵ), salt bridge (1.80ϵ), hydrogen bond among backbones (5.00ϵ), and hydrogen bond between polar side chains and backbones (2.50ϵ). The temperature is in the unit of ϵ/k_B, where k_B is the Boltzmann constant (14, 18).

For each peptide system at each temperature, we performed a DMD simulation for 10^6 time units (*tu*). Here *tu* is a reduced time unit that was derived from the units of mass, energy, and length. The length of the DMD simulations was chosen to be long enough so that equilibrium was observed for all studied peptide systems. We assumed that equilibrium was achieved in each simulation when the distribution of potential energies sampled along each trajectory did not change further with the simulation time. Overall, we performed 46 DMD simulations of trimers and 22 DMD simulations of hexamers.

Trimer Folds into a Coiled-coil State at Low Temperatures—To quantify the structural transitions that occur in a system of three ccβ peptides, we calculated their propensities to form secondary structure elements, α-helices and β-strands, at different temperatures, using a method proposed by Srinivasan and Rose (27) (Fig. 1). Briefly, at each temperature the secondary structure propensities of each residue were calculated and averaged over the corresponding equilibrium trajectory. Then the secondary structure propensities of the peptides were computed as the average over all the residues. We did not include in the plot (Fig. 1) the propensity of forming turns and random coils. We found that at low temperatures these peptides favor α-helical states. The α-helix to β-strand transition occurs at the temperature $T_c \approx 0.71$. At high temperatures, $T > 0.71$, the peptides adopt β-strands, in agreement with the experiments (7).

At temperatures $T < T_c \approx 0.71$, we observed the formation of the coiled-coil trimers with low potential energies (Fig. 2, *A* and *B*). We observed two types of coiled-coil ccβ trimers as follows. (i) Three helices orient in the same direction as determined in the experiment (type I, Fig. 2*A*). (ii) The orientation of one of the peptides is opposite that of the other two peptides (type II, Fig. 2*B*). The type I trimer was strikingly similar to the experimental native state structure (Protein Data Bank code 1s9z); the root mean square distance (r.m.s.d.) between a low energy type I and the experimental structure was 1.26 Å (Fig. 2*C*). Type I and II structures were the result of the orientation permutations of the three peptides in a coiled-coil trimer. Because of the simplifications of the protein structure used in our simulations, these two structures were indistinguishable. The potential energies of the two coiled-coil states were approximately the same in DMD simulations, although in some simulations the potential energy of the type II (non-native) state was even lower than that of the type I (native) state. To determine the thermodynamic viability of the two folded coiled-coil states, we performed free energy calculations on these states using all-atom molecular dynamics simulations.

We first reconstructed the all-atom representation of the two coiled-coil structures from the coarse-grained representation (see "Materials and Methods"). We then performed 2-ns all-atom molecular dynamics simulations of the two typical trimers, obtained in DMD simulations, in the presence of explicit water molecules. The r.m.s.d. between the initial and final ccβ trimer states is smaller than 2 Å, suggesting that there is no significant conformational drift in the process of the 2-ns molecular dynamics simulations. We calculated different terms of the conformational free energy for the two states by using MM/PBSA (molecular mechanics/Poisson-Boltzmann solvent-accessible surface area) (TABLE ONE) (see "Materials and Methods"). Because the unfolded states of the two types of trimers are the same, comparing their conformational free energy was equivalent to comparing their stability. We found that the free energy of the native-like state is 21 kcal/mol lower than that of the non-native trimer. Although the free energy difference between these two conformational states was within their standard deviations, the difference between their average values was still statistically significant, with a p value smaller than 10^{-16} (according to Student's t test). Therefore, the native conformation was indeed more stable than the non-native one.

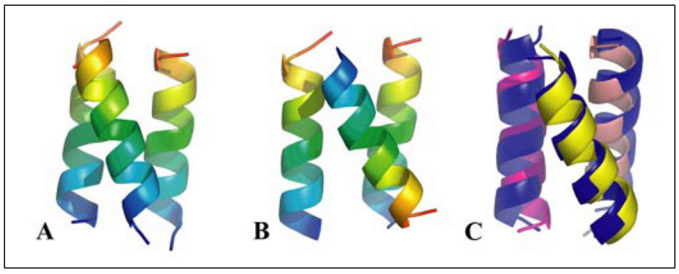

FIGURE 2. **Two types of coiled-coil structures observed in low temperature simulations.** *A*, the three monomers orient toward the same direction; *B*, one of the ccβ peptides is oriented in the opposite direction than the other two peptides. The monomer peptides in *A* and *B* are colored from *green* (N terminus) to *red* (C terminus). *C*, the structural alignment of the experimental trimer (Protein Data Bank code 1s9z; colored in *blue*) and one of the native-like coiled-coil trimers obtained in simulations. The r.m.s.d. between the experimental and simulation structures is 1.26 Å.

High Temperature Promotes the Formation of β-Sheet Rich Aggregates—At high temperatures ($T > 0.71$), we observed β-rich aggregates formed by three ccβ peptides (Fig. 1). We observed the following two types of aggregate structures: (i) β-hairpin aggregates (Fig. 3*A*), which comprise individual β-hairpin-shaped peptides; and (ii) coiled β-sheets (Fig. 3*B*), in which peptides collectively form β-sheets that coil around a central region with packed hydrophobic residues inside. The hydrophobic residues in a coiled β-sheet aggregate are clustered inside the core, whereas the polar residues are exposed to solvent (Fig. 3*C*). The aggregates are stabilized by hydrophobic packing, hydrogen bonds, and salt bridges between the oppositely charged residues. As with our low temperature studies, our coarse-grained model cannot distinguish these two types of aggregates. Thus, we performed molecular mechanics free energy calculations to estimate the thermodynamic viability of the two aggregate structures.

We reconstructed the all-atom representation of the coarse-grained aggregates from DMD simulations ("Materials and Methods"). Following the same protocol described above, we calculated the conformational free energies of the two aggregates, which are listed in TABLE ONE. Because the reference states were identical, the difference between the conformational free energies $\Delta\Delta G$ discriminates the two putative aggregation states. We found that the conformational free energy of the coiled β-sheet aggregate was ~55 kcal/mol lower than that of the β-hairpin aggregate. This difference was statistically significant because the standard deviations of the two values do not overlap. Therefore, the coiled β-sheet aggregate was thermodynamically more stable than the β-hairpin aggregate, and we proposed it as the putative building block of the large scale amyloid fibril. This model of the aggregate is in agreement with the experimental observation in that there are no intra-peptide hydrogen bonds (7), which exist in the β-hairpin aggregates (Fig. 3*A*).

TABLE ONE

The conformational free energy of various structures in the folded and aggregated states

The energy terms are in kcal/mol units, and their standard deviations are presented. The energy terms are introduced under "Materials and Methods."

Trimer		E_{GAS}			G_{SOL}		$-TS$	G_{conf}
		E_{ELE}	E_{VDW}	E_{INT}	G_{PB}	G_{SUR}		
Low temperature	Native	−2989 ± 54	−160.2 ± 11.5	1050.3 ± 21.9	−1402 ± 58	25.04 ± 0.47	−586.4	−4062 ± 22
	Non-native	−3175 ± 58	−135.6 ± 11.6	1030.8 ± 22.5	−1211 ± 53	26.39 ± 0.52	−576.8	−4041 ± 22
High temperature	Coiled	−2928 ± 53	−142.4 ± 11.2	1046.1 ± 22.3	−1396 ± 51	26.12 ± 0.49	−582.3	−3976 ± 21
	Hairpin	−3118 ± 60	−143.3 ± 11.4	1070.0 ± 22.4	−1175 ± 50	25.33 ± 0.51	−579.6	−3921 ± 24

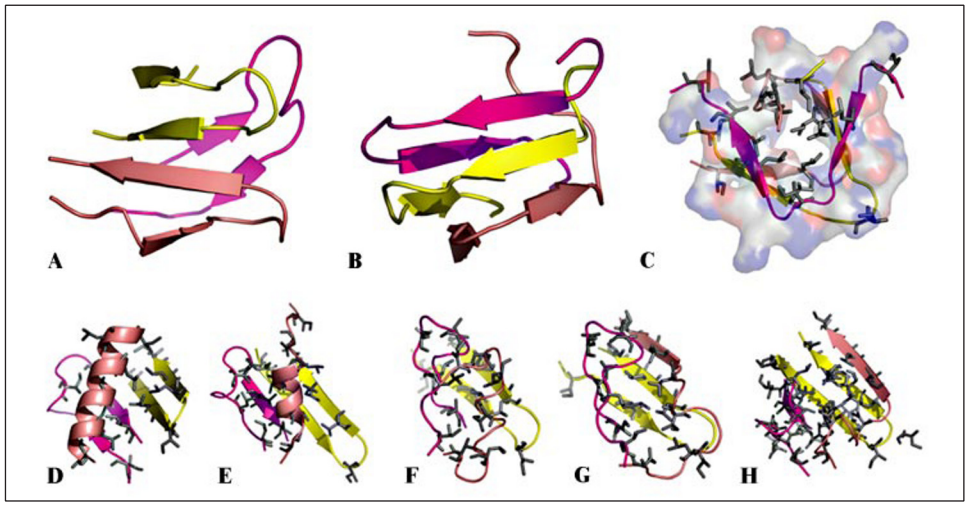

FIGURE 3. **Two typical structures of the β-rich aggregates at high temperatures.** *A,* β-hairpin aggregate, where individual peptides form β-hairpins; *B,* a coiled β-strand aggregate, in which individual peptides form β-sheets with each other and are coiled around the center. In both aggregates, the structure is stabilized by packing the hydrophobic residues inside and solvating the polar residues outside. *C,* the top view of the coiled β-strand aggregate presented in *B*. The hydrophobic residues are in *stick* representation and are colored *gray*, and the polar residues are shown by their solvent-exposed surfaces colored according to their polar atoms (*blue* for nitrogen and *red* for oxygen). The snapshots during a typical α-helix to β-sheets transition are as follows: 2.29×10^5 *tu* (*D*), 2.62×10^5 *tu* (*E*), 2.64×10^5 *tu* (*F*), 2.68×10^5 *tu* (*G*), and 2.76×10^5 *tu* (*H*).

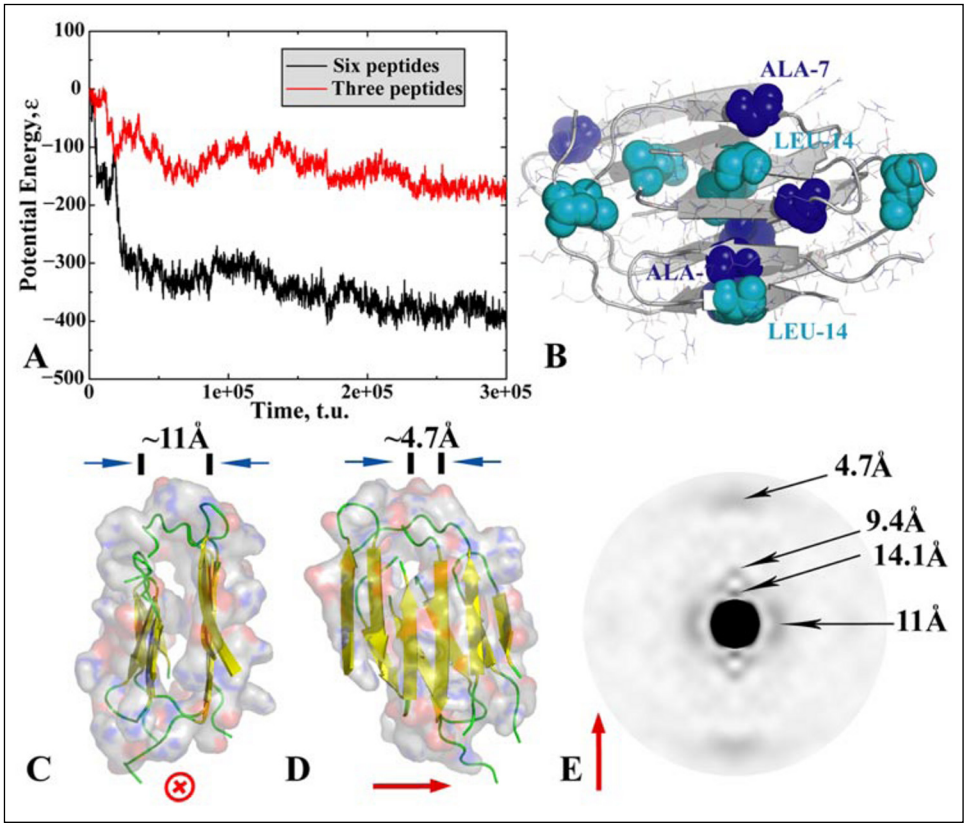

FIGURE 4. **Aggregation of six peptides.** *A,* plot of potential energy *versus* time for a three-peptide simulation and for a six-peptide simulation (both resulting in aggregates). Only the first 3×10^5 *tu* simulations are shown, and potential energies do not change in the following simulation trajectories. *B,* typical hexamer aggregate with all residues shown as *sticks* except for the hydrophobic Leu-14 (*cyan*) and Ala-7 (*dark blue*). These two residues were identified in experiments (7) as having a high propensity to form intermolecular hydrogen bonds. *C* shows the top and *D* shows the side views of the aggregate. The polar residues are shown in surface representations, and the backbones are shown in a schematic. The *red arrows* indicate the putative long axis of the fibril. The simulation results indicate that the aggregates form the characteristic double β-sheet structures. The hydrogen bonds in the β-sheets are aligned along the fibril axis. The separation between the two neighboring β-sheets is ~11 Å. The calculated x-ray diffraction pattern (*E*) confirms the two periodicities and agrees with experiments. Because of the finite size effect, we also find peaks corresponding to $4.7 \times 2 = 9.4$ Å and $4.7 \times 3 = 14.1$ Å along the fibril axis.

A Preformed β-Sheet Accelerates the Conversion from α-Helixes to β-Strands—At temperatures $T > T_c \approx 0.71$, β-sheets are thermodynamically more stable than α-helices (Fig. 1). Although in the vicinity of the transition temperature, $T_c \approx 0.71$, the free energy difference between the two states of a ccβ peptide (a β-sheet and an α-helix) was marginal, there was a large free energy barrier separating these two conformational states (9). Thus, the inter-conversion of an isolated α-helix to a stable β-sheet was a rare event, in accord with Ding *et al.* (9). Here we examined the α-helix to β-sheet transition during aggregation near the transition temperature $T_c \approx 0.71$. In Fig. 3, *D–H,* we presented a series of snapshots during a typical transition observed in DMD simulations at $T = 0.725$. Initially, hydrophobic interactions drove a kinetically trapped α-helix to bind to a pre-formed stable β-sheet; the exposed hydrophobic surface of the β-sheet interacted with the hydrophobic face of the amphipathic helix (Fig. 3*D*). This interaction was because of an attractive term between hydrophobic residues, which mimics the solvent effect. The α-helix then melts into an unstructured state that was stabilized by forming additional hydrophobic contacts with the external surface of the pre-formed β-sheet partner; this is similar to the hydrophobic solid surface-induced unfolding of α-helices (28). These additional hydrophobic contacts between the peptide and the pre-formed β-sheet greatly reduced the available conformations of the random coil state and, thus, the entropy of the chain. However, the enthalpic gain because of the newly formed hydrophobic interactions overwhelmed the loss of entropy, so that the free energy barrier of the α-helix to β-sheet inter-conversion was reduced. Hence, the "templated" transition time in simulations (Fig. 3, *D–F*; snapshots taken

at 2.29×10^5, 2.62×10^5, and 2.64×10^5 time units, respectively) was on the order of 10^4 *tu*, which is smaller than the transition time of 10^5–10^6 *tu*, typical of an isolated peptide (9).

Most interestingly, the increase of the local kinetic energy during the melting process of the α-helix leads to local overheating of the thermal bath, which results in partial melting of the proximal β-strands of the ccβ peptide (Fig. 3, *E* and *F*). When the local overheating dissipates due to the thermal bath equilibration, the partially melted β-strands refold (Fig. 3*H*), resulting in a β-sheet amyloid aggregate precursor.

Six Peptides Form a Fibril-like Aggregate—To study further the propagation of the ccβ peptide aggregation, we performed DMD simulations of six peptides at elevated temperatures $T > 0.71$ (Fig. 4*A*). Starting from fully extended conformations that are spatially separated, all peptides rapidly equilibrated as did the isolated peptides (Fig. 4*A*). The equilibration process resulted in a continuous decrease of the potential energy during the first half of 10^4 *tu*. Because of the diffusion of the peptides in the simulation box, there was a short plateau of the potential energy in the following 10^4 *tu*. The potential energy of the system then sharply decreased as a result of nonspecific association of ccβ peptides driven by the hydrophobic interactions. A slow conformational rearrangement from this initial ccβ peptide assembly leads to an ordered aggregate (Fig. 4*B*) and is accompanied by a slow decrease of the average potential energy and large potential energy fluctuations. To compare the three peptide and six peptide ccβ simulations, in Fig. 4*A* we also present a typical simulation trajectory of three ccβ peptides at the same temperature. Although the general trends of potential energy trajectories for these two systems were similar, the potential energy of the final hexamer aggregate was lower than twice the energy of the trimer aggregate. The extra stabilization of the ccβ hexamer with respect to the trimer agreed with the hyperstability of amyloid fibrils. Next we examined the structural properties of the ordered aggregate obtained in DMD simulations.

We present a typical aggregate structure that comprises six ccβ peptides in Fig. 4*B*. The aggregates mainly consisted of anti-parallel β-strands. Because our simplified DMD force field does not distinguish between β-hairpins and coiled-strands, as discussed above, we observed a mixture of these two types of β-structures, similar to the observed trimer aggregates. We found that residues Ala-7 and Leu-14 have a high probability to form hydrogen bonds (Fig. 4*B*), in accordance with the experiments (7). The aggregates have the characteristic cross-β-structure (Fig. 4, *C* and *D*); the aggregates were formed by packing β-sheets against each other with hydrogen bonds in the β-sheets aligned along the fibril axis. The distance between the β-strands in the β-sheets was 4.7 Å, which is the typical hydrogen bond distance (Fig. 4*D*). The distance between packed β-sheets is ~11 Å (Fig. 4*C*).

We further computed the x-ray diffraction pattern of the aggregate as described by Ding *et al.* (29) (Fig. 4*E*). The x-ray pattern featured the two signature distances of amyloid fibrils, in agreement with the experimental diffraction pattern of the ccβ aggregates (7). The only difference between the experimental and simulation x-ray diffraction pattern was the absence of the doublet of 11 Å along the equatorial axis (perpendicular to the fibril axis). In experiments, this doublet peak was interpreted as the distance between more than two sheets packed against each other (7). Because of the limited number of peptides in our simulations, we did not observe such a large scale aggregate structure. However, we did expect to observe this 22 Å peak in a larger system.

DISCUSSION

The ccβ peptide was designed *de novo* to fold into a coiled-coil native state at low temperatures and aggregate into amyloid fibrils at elevated temperatures. Experimental studies of ccβ peptides (7) provide important checkpoints for computational modeling of protein dynamics. We employ a recently developed simplified protein model (18) to study the folding and aggregation of ccβ peptides. Because of its coarse-grained nature, our simplified protein model has a degenerate free energy landscape. For example, we observe a non-native coiled-coil state at low temperatures and the coexistence of ccβ-hairpin and coiled β-sheet aggregates at elevated temperatures. By coupling traditional all-atom molecular mechanics simulations with the rapid DMD simulations of simplified protein models, we eliminate free energy landscape degeneracies by screening for the thermodynamically viable states in all-atom molecular mechanics simulations. Such an approach allows the sampling of large protein conformational spaces while maintaining the accuracy of atomic resolution.

With our methodology, we successfully reproduce the folding and aggregation dynamics of the ccβ peptides, including the temperature dependence of its folding and aggregation behavior. By using all-atom free energy calculations to filter out the degenerate states from the coarse-grained protein model simulations, we select the coiled-strand β-sheet aggregates as the most probable aggregation states. We postulate that the larger ccβ peptide aggregates are mainly composed of coiled-strand β-structures.

The conformational transition from α-helices to β-sheets is an obligatory step toward amyloid fibril formation from natively α-rich proteins, such as prion proteins in prion diseases and Aβ peptides in Alzheimer disease (4). The ability of the ccβ peptide to feature both α-helix and β-strand conformations (7) enables us to study such secondary structure transitions. In simulations we observe a temperature-dependent transition from α-helix to β-strand with a midpoint temperature $T_c \approx 0.71$. At $T \approx T_c$, conformations of α-helices and β-strands have a marginal free energy difference so that an unfolded peptide can adopt either conformation. The secondary structure transition of an isolated α-helix peptide is often difficult to observe (9) because of the large free energy barrier between α-helices and β-sheets. In our simulations, we find that this free energy barrier is reduced by interaction with a preformed β-sheet with an exposed hydrophobic surface and unsaturated hydrogen bonds. Unsaturated hydrogen bonds near the edges of the pre-formed β-sheets greatly stabilize the newly formed β-sheet. Thus, the conformation change of an isolated α-helix peptide into a β-structure appears to be substantially promoted when other β-sheet peptides are introduced into the system (9). Our simulations provide computational evidence in support of the template-mediated aggregation mechanism of prion proteins proposed by Prusiner (3). Our study suggests a generic scenario of the prion-like infectivity of protein misfolding, wherein infected particles expose hydrophobic surfaces and backbone hydrogen bond donors/acceptors that alter the free energy landscape of the normal proteins. This exposure reduces the free energy of both the barrier and the aggregates with respect to the native state.

The aggregate structures obtained in our DMD simulations contain the cross-β-patterns observed in amyloid fibrils. In addition, the computed x-ray fibrillar diffraction pattern agrees with the experimental data (7). Kammerer *et al.* (see Fig. 4 in Ref. 7) proposed a structural model of ccβ peptide amyloid fibril, in which individual ccβ peptides are in an extended β-strand conformation forming anti-parallel β-sheets along the fibril axis. The hydrophobic residues in a β-sheet form two clusters separated by the β-sheet plane (see Fig. 4 in Ref. 7). These β-sheets pack against each other, stabilized by hydrophobic interactions and by a set of buried polar residues that form salt bridges. It is questionable whether this model proposed by Kammerer *et al.* (7) is thermodynamically viable because burying polar residues is energetically unfavorable. In our model, individual peptides form β-strands coiled

around their center instead of extended, stacked β-strands. Thus, the hydrophobic residues can cluster together without burying charged residues (Figs. 3*C* and 4*B*). Because of the limited number of peptides studied in our simulations, the size of the aggregate model does not reach the dimensions that can be used for comparing with atomic force microscopy measurements (7). We postulate that our prefibrillar aggregates, upon further assembly, would result in the large scale amyloid fibrils observed in experiments.

REFERENCES

1. Hardy, J., and Selkoe, D. J. (2002) *Science* **297,** 353–356
2. Sunde, M., Serpell, L. C., Bartlam, M., Fraser, P. E., Pepys, M. B., and Blake, C. C. F. (1997) *J. Mol. Biol.* **273,** 729–739
3. Prusiner, S. B. (1998) *Proc. Natl. Acad. Sci. U. S. A.* **95,** 13363–13383
4. Kirkitadze, M. D., Condron, M. M., and Teplow, D. B. (2001) *J. Mol. Biol.* **312,** 1103–1119
5. Guijarro, J. I., Sunde, M., Jones, J. A., Campbell, I. D., and Dobson, C. M. (1998) *Proc. Natl. Acad. Sci. U. S. A.* **95,** 4224–4228
6. Fandrich, M., Fletcher, M. A., and Dobson, C. M. (2001) *Nature* **410,** 165–166
7. Kammerer, R. A., Kostrewa, D., Zurdo, J., Detken, A., Garcia-Echeverria, C., Green, J. D., Muller, S. A., Meier, B. H., Winkler, F. K., Dobson, C. M., and Steinmetz, M. O. (2004) *Proc. Natl. Acad. Sci. U. S. A.* **101,** 4435–4440
8. Peng, Y., and Hansmann, U. H. E. (2003) *Phys. Rev. E. Stat. Nonlin. Soft. Matter Phys.* **68,** 041911–041917
9. Ding, F., Borreguero, J. M., Buldyrev, S. V., Stanley, H. E., and Dokholyan, N. V. (2003) *Proteins Struct. Funct. Genet.* **53,** 220–228
10. Peng, S., Ding, F., Urbanc, B., Buldyrev, S. V., Cruz, L., Stanley, H. E., and Dokholyan, N. V. (2004) *Phys. Rev. E. Stat. Nonlin. Soft. Matter Phys.* **69,** 041908–041914
11. Urbanc, B., Cruz, L., Ding, F., Sammond, D., Khare, S., Buldyrev, S. V., Stanley, H. E., and Dokholyan, N. V. (2004) *Biophys. J.* **87,** 2310–2321
12. Lipfert, J., Franklin, J., Wu, F., and Doniach, S. (2005) *J. Mol. Biol.* **349,** 648–658
13. Malolepsza, E., Boniecki, M., Kolinski, A., and Piela, L. (2005) *Proc. Natl. Acad. Sci. U. S. A.* **102,** 7835–7840
14. Dokholyan, N. V., Buldyrev, S. V., Stanley, H. E., and Shakhnovich, E. I. (1998) *Folding Des.* **3,** 577–587
15. Zhou, Y. Q., Karplus, M., Wichert, J. M., and Hall, C. K. (1997) *J. Chem. Phys.* **107,** 10691–10708
16. Ding, F., and Dokholyan, N. V. (2005) *Trends Biotechnol.* **23,** 450–455
17. Dokholyan, N. V., Borreguero, J. M., Buldyrev, S. V., Ding, F., Stanley, H. E., and Shakhnovich, E. I. (2003) *Methods Enzymol.* **374,** 616–638
18. Ding, F., Buldyrev, S. V., and Dokholyan, N. V. (2005) *Biophys. J.* **88,** 147–155
19. Dunbrack, R. L., Jr., and Cohen, F. E. (1997) *Protein Sci.* **6,** 1661–1681
20. Hermans, J., Berendsen, H. J. C., Vangunsteren, W. F., and Postma, J. P. M. (1984) *Biopolymers* **23,** 1513–1518
21. Lazaridis, T., and Karplus, M. (1999) *Proteins Struct. Funct. Genet.* **35,** 133–152
22. Kortemme, T., Morozov, A. V., and Baker, D. (2003) *J. Mol. Biol.* **326,** 1239–1259
23. Pearlman, D. A., Case, D. A., Caldwell, J. W., Ross, W. S., Cheatham, T. E., Debolt, S. E., Ferguson, D. M., Seibel, G. L., and Kollman, P. A. (1995) *Comput. Phys. Commun.* **91,** 1–41
24. Berendsen, H. J. C., Postma, J. P. M., Vangunsteren, W. F., DiNola, A., and Haak, J. R. (1984) *J. Chem. Phys.* **81,** 3684–3690
25. Kollman, P. A., Massova, I., Reyes, C., Kuhn, B., Huo, S. H., Chong, L., Lee, M., Lee, T., Duan, Y., Wang, W., Donini, O., Cieplak, P., Srinivasan, J., Case, D. A., and Cheatham, T. E. (2000) *Acc. Chem. Res.* **33,** 889–897
26. Vorobjev, Y. N., and Hermans, J. (1997) *Biophys. J.* **72,** MP459
27. Srinivasan, R., and Rose, G. D. (1999) *Proc. Natl. Acad. Sci. U. S. A.* **96,** 14258–14263
28. Sethuraman, A., and Belfort, G. (2005) *Biophys. J.* **88,** 1322–1333
29. Ding, F., Dokholyan, N. V., Buldyrev, S. V., Stanley, H. E., and Shakhnovich, E. I. (2002) *J. Mol. Biol.* **324,** 851–857